The Journal of Experimental Biology 213, 2665-2672

doi:10.1242/jeb.043216

Harbor seal vibrissa morphology suppresses vortex-induced vibrations

Wolf Hanke[1], Matthias Witte[2], Lars Miersch[1], Martin Brede[2], Johannes Oeffner[1], Mark Michael[2], Frederike Hanke[1], Alfred Leder[2], and Guido Dehnhardt[1,*]

[1]Institute for Biosciences, Department of Sensory and Cognitive Ecology, Marine Science Center, University of Rostock, 18059 Rostock, Germany and [2]Faculty of Engineering, Department of Fluid Mechanics, University of Rostock, 18059 Rostock, Germany

*Author for correspondence (guido.dehnhardt@uni-rostock.de)

Accepted 26 April 2010

SUMMARY

Harbor seals (*Phoca vitulina*) often live in dark and turbid waters, where their mystacial vibrissae, or whiskers, play an important role in orientation. Besides detecting and discriminating objects by direct touch, harbor seals use their whiskers to analyze water movements, for example those generated by prey fish or by conspecifics. Even the weak water movements left behind by objects that have passed by earlier can be sensed and followed accurately (hydrodynamic trail following). While scanning the water for these hydrodynamic signals at a swimming speed in the order of meters per second, the seal keeps its long and flexible whiskers in an abducted position, largely perpendicular to the swimming direction. Remarkably, the whiskers of harbor seals possess a specialized undulated surface structure, the function of which was, up to now, unknown. Here, we show that this structure effectively changes the vortex street behind the whiskers and reduces the vibrations that would otherwise be induced by the shedding of vortices from the whiskers (vortex-induced vibrations). Using force measurements, flow measurements and numerical simulations, we find that the dynamic forces on harbor seal whiskers are, by at least an order of magnitude, lower than those on sea lion (*Zalophus californianus*) whiskers, which do not share the undulated structure. The results are discussed in the light of pinniped sensory biology and potential biomimetic applications.

Supplementary material available online at http://jeb.biologists.org/cgi/content/full/213/15/2665/DC1

Key words: harbor seal, pinniped, vibrissae, hydrodynamics, PIV, CFD.

INTRODUCTION

Whiskers, also known as vibrissae or sinus hairs, are tactile hairs present in almost all mammals. The most prominent whiskers are usually found on the snout (mystacial vibrissae) and above the eyes, but also the legs, feet or other parts of the body can bear vibrissae. Vibrissae are generally longer and stiffer than normal body hairs, and their follicles are surrounded by complex blood sinuses and an ample variety of mechanoreceptors [Struton strakes (cf. Dehnhardt et al., 1999; Ebara et al., 2002)]. Besides the use of vibrissae for the haptic examination of objects (active touch) (Dehnhardt and Kaminski, 1995; Hartmann, 2001), their use by aquatic and semiaquatic mammals for sensing and analyzing water flow has recently come into focus (Catania et al., 2008; Dehnhardt, 2002; Dehnhardt et al., 1998a; Dehnhardt et al., 2001; Dehnhardt et al., 1998b; Schulte-Pelkum et al., 2007).

Harbor seals (*Phoca vitulina* L.) use their mystacial vibrissae to identify objects by active touch and for sensing water movements caused by prey fish or by other seals (Dehnhardt and Kaminski, 1995; Dehnhardt et al., 1998a; Dehnhardt et al., 2001; Hanke and Bleckmann, 2004; Hanke et al., 2000; Schulte-Pelkum et al., 2007). They are able to follow the path of these water disturbances over a distance that can by far surpass the range of vision or hearing (hydrodynamic trail following). While swimming and scanning the water for flow patterns, harbor seals keep their whiskers in an abducted position, largely perpendicular to the swimming direction. However, the flexible vibrissae bend easily, and the mechanoreceptors at the follicle are sensitive to displacements of the hair of 1 μm or less at their best frequencies (Dehnhardt et al., 1998a). These findings raised the question concerning how harbor seals cope with the flow resistance on their vibrissae and with vortex-induced vibrations (VIVs) – that is, the oscillations due to vortex shedding that occur when an object is dragged through the water.

We suspected the solution might reside in the morphology of the hair. The whiskers of harbor seals and most other members of the phocid family have a peculiar cross-sectional shape: the cross-section is elliptical, and the ratio of the major and minor axes changes along the hair, with a period of approximately 1 to 3 mm, thus giving the flattened hair an undulated surface structure (Fig. 1A,B) that distinguishes it from the vibrissae of eared seals (*Otariidae*) such as the sea lion (Fig. 1C,D). In this study, we investigated the hydrodynamic function of this undulated structure in the live animal by means of a head-mounted camera, in the isolated free vibrissa using piezoelectric force transducers, in a short piece of vibrissa using micrometer-scale stereoscopic particle image velocimetry (micro-stereo-PIV) and with computational fluid dynamics (CFD).

MATERIALS AND METHODS

Head-mounted camera

A head-mounted camera (HMC) system was designed for the specific needs of recording the posture and movements of the vibrissae of a harbor seal during a hydrodynamic trail-following task. An analogue CCD camera module (Conrad Electronics, Hirschau, Germany) with an 8 mm lens in a waterproof acrylic housing was attached to the eye-mask worn by the seal (Fig. 2B). The images from the camera (for an example, see Fig. 2B) were recorded by a flash memory Mpeg4 recorder with an analog-to-digital converter that was mounted in a waterproof plastic housing

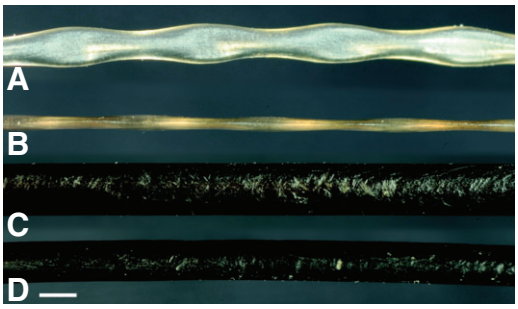

Fig. 1. Structure of harbor seal (*Phoca vitulina*) and California sea lion (*Zalophus californianus*) vibrissae. (A,B) Harbor seal vibrissa in dorsal (A) and frontal view (B). The vibrissa is flattened in the dorso-ventral direction and possesses an undulated structure. (C,D) Sea lion vibrissa in frontal (C) and dorsal view (D). The vibrissa is slightly flattened and does not possess an undulated structure. Scale bar: 1 mm.

and attached to the back of the seal by means of a harness (see supplementary material Fig. S1A).

Animal training and behaviour

To ensure that the animal was operating in the hydrodynamic detection mode and thus positioned its whiskers accordingly, it was trained to follow the path of a miniature submarine (compare supplementary material Fig. S1B–D). The animal was trained to wait at a station (Fig. 2A) wearing an eye-mask and headphones with pink noise that masked the noise from the engine of the submarine while the submarine generated a hydrodynamic trail. After the engine was switched off, the headphones were removed from the seal, and the seal set out to find the submarine by following its hydrodynamic trail. During this task, the position and movement of the whiskers were recorded with the HMC system.

All videos recorded by the HMC system were reviewed and evaluated qualitatively. In cases where no relative movements of the camera head and the snout of the seal were observed, videos were evaluated by superimposing images to detect vibrissal movements.

Vibration measurements of single vibrissae in a rotation flume

The rotation flume consisted of a round tank with a diameter of 124 cm, filled with water to a level of 20 cm. The tank rotated around its vertical axis, leading to a rotation of the water, with the tank at a constant angular speed after a break-in period. Angular speed was monitored with an optical sensor. Above the tank, a movable holder was mounted that allowed the immersion of a vibrissa into the water at a variable distance from the axis of rotation (and thus at variable flow speed with no additional break-in period). Three harbor seal vibrissae of different sizes were obtained from a juvenile animal that had died from natural causes in the Research Center Büsum (University of Kiel, Germany). Three sea lion vibrissae of matching lengths (difference 10% or less) were supplied by the Natural History Museum Münster, Germany. One vibrissa at a time was mounted in a piezoceramic transducer shaped as a hollow cylinder. The piezoceramic transducer was connected to a charge amplifier that output a voltage proportional to the force on the transducer. The charge amplifier output was recorded and analysed using LabView (National Instruments, Austin, Texas, USA). This way, relative measures of the momenta on the test vibrissae were obtained.

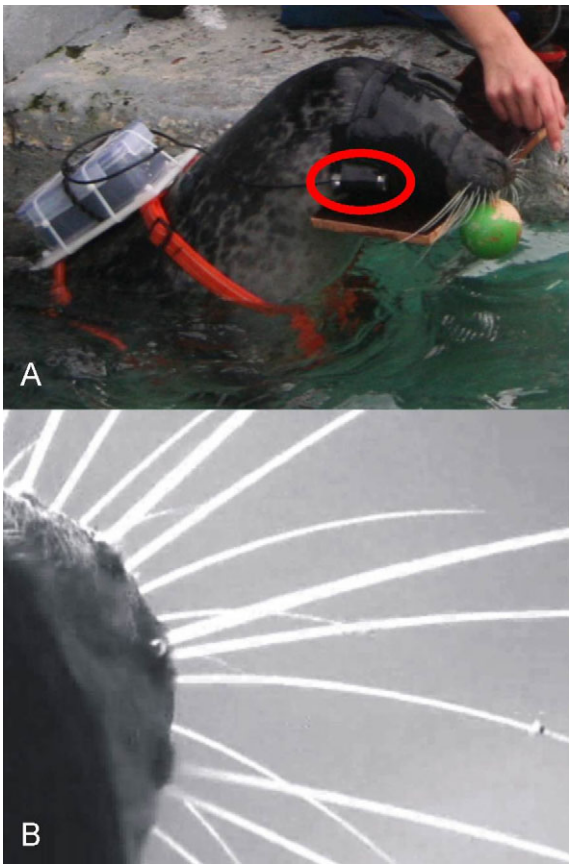

Fig. 2. Head-mounted camera. (A) Position of the head-mounted camera (red ellipse) fixed to the eye-mask that the seal is wearing. The head-mounted camera monitored the position and movements of the whiskers while the seal performed a hydrodynamic trail-following task. The seal is stationing at a platform with a ball target for the photograph. (B) View from the head-mounted camera under water, showing the posture of the vibrissae.

Micro-stereo particle image velocimetry

Particle image velocimetry (PIV) analyzes the movements of neutrally buoyant particles that are added to the flow and filmed in selected layers (Adrian, 1991). The layers can be selected by illuminating the particles only within a thin laser-light sheet in the macroscopic case or by choosing the depth of focus appropriately in the microscopic case (Nguyen and Wereley, 2002). The experimental setup was implemented using a stereo microscope with two optical paths through a single lens (Brede et al., 2006). The third velocity component (z-component, out-of-plane component) was obtained from a stereoscopic PIV approach (Prasad and Adrian, 1993). A vibrissa section of length 15 mm was placed in a closed-loop water channel with a cross-section of $15\times30\,mm^2$, orthogonal to the flow, corresponding to the natural posture in the swimming seal. The observation area in the plane orthogonal to the vibrissa axis (x–y plane, compare Fig. 3) covered 1.65 mm×2.55 mm. A Zeiss Stemi 11 stereo microscope (Zeiss, Jena, Germany) with two optical paths through a single lens (Leica planapo 2.0) was used for the observation of the flow. Two HiSense PIV cameras (Dantec Dynamics, Copenhagen, Denmark) generated a double-frame image pair. The flow-field was completely illuminated using a pulsed 5 W LED. The water was seeded with polyamide particles, of diameter

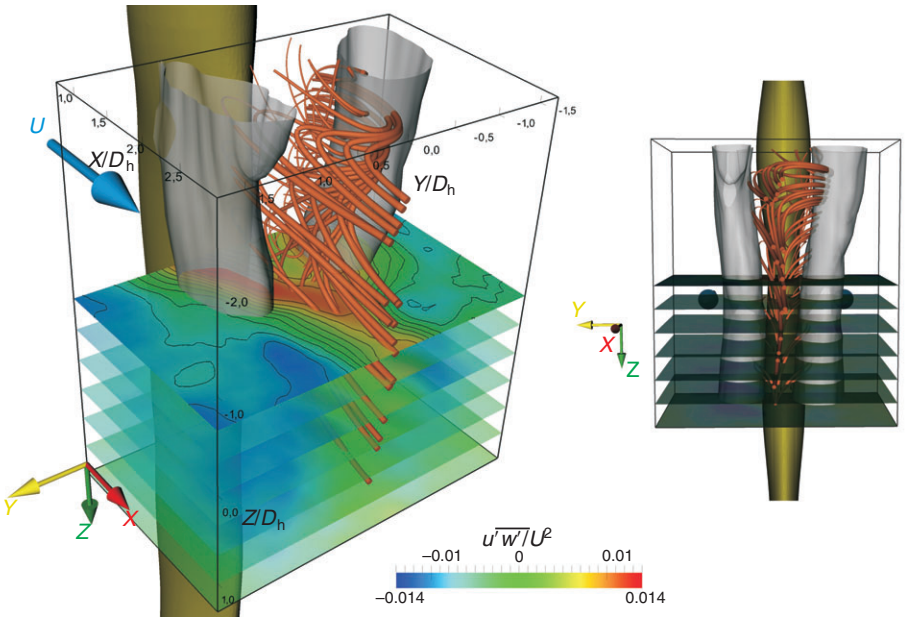

Fig. 3. Two views of the time-averaged velocity field (total of 500 measurements at random phases of the flow) obtained from micro-stereo-PIV measurements in the wake of a vibrissa of a harbor seal, coordinates normalized with the hydraulic diameter of the vibrissa D_h. Three-dimensional streamline reconstruction from a 13-plane velocity field. Grey isosurfaces: vortex core detection using the λ_2 vortex criterion (Jeong and Hussain, 1995). Color: Reynolds shear stress $\overline{u'w'}/U^2$. Colored horizontal planes (and, on the right, grey horizontal planes) depict the spacing of the measurement planes. U is the velocity of the incoming flow; u, v and w are the velocities in the x, y and z direction, respectively.

5 µm. Particle images could then be observed within the focal plane of the microscope. The two in-plane velocity vector components were calculated using a standard cross-correlation scheme with an interrogation area size of 32×32 pixels and an overlap of 50%. The third velocity vector component (out-of-plane component) was obtained from a stereoscopic vector field evaluation, with a correlation depth of approximately 60 µm.

Numerical simulation (computational fluid dynamics)

Stereo-micro-PIV is a suitable technique to observe the three-dimensional (3-D) velocity field on a two-dimensional focal plane. The limitation of this method results from the fact that measurements in different planes are not performed simultaneously. To obtain a volumetric reconstruction (Fig. 3), the unsteady velocity snapshots on each plane had to be time averaged. The disadvantage of this method is that no information about the spatial structure of the unsteady flow is available. Therefore, numerical computations CFD were performed in addition to the measurements.

The bases for the CFD simulations are the equation of motion (the Navier–Stokes equation) and the continuity equation. The equation system was solved numerically using the direct numerical simulation (DNS) approach with the parameters given in the Supplementary Information (supplementary material Fig. S2 and Fig. S2 legend). We chose the library openFOAM (GPL) (OpenCFD, Caversham, Reading, UK) as a numerical solver owing to its capability to solve partial differential equations on parallel computer architectures. The discretization of the governing equations was based on the finite-volume method.

For the spatial discretization and time integration, only second-order schemes were used. To obtain the characteristic 3-D surface structure of the vibrissae for the CFD analysis, 80 ripples of natural vibrissae were analyzed by photogrammetry. The resulting main geometric parameters were used to create an idealized vibrissa surface model.

The validity of the simulation method as well as the grid independency were confirmed by calculating the wake of a circular cylinder at a Reynolds number (Re) of 500 and performing a detailed comparison with numerical and experimental data from various sources (Balachandar et al., 1997; Brede et al., 1996; Leder, 1991; Zdravkovich, 1995; Zdravkovich, 2003). The results were in very good agreement with the literature concerning the Strouhal number, separation angle and Reynolds stresses of the flow.

RESULTS

A head-mounted camera (Fig. 2A, ellipse) was used in order to assess the position and movements of the vibrissae under water at typical swimming speeds of 0.5 to 1 m s^{-1} while the blindfolded harbor seal solved a hydrodynamic perception task in which it had to follow the wake of a miniature submarine (Dehnhardt et al., 2001). The recordings from the head-mounted camera during swimming (Fig. 2B) showed no discernible difference in the posture of the vibrissae compared with the situation in air. The vibrissae did not markedly bend backwards during forward swimming, nor did they vibrate in the flow to a degree that was resolved by the video system – that is, any unresolved vibration amplitude was clearly below 0.2 mm at 1 m s^{-1} swimming speed.

The reduction of vibration found on the organismic level was further investigated at the level of single vibrissae by assessing their vibration amplitude and frequency in a rotational flow tank. One vibrissa at a time was mounted in the flow, with its base fit into a piezoelectric transducer shaped as a hollow cylinder. The piezoelectric transducer was attached to a charge amplifier that output a voltage proportional to the force acting on the transducer. Three vibrissae of a harbor seal (*Phoca vitulina*) and three vibrissae of a California sea lion (*Zalophus californianus*) were tested at different flow speeds ranging from 0.323 m s^{-1} to 0.550 m s^{-1}. The vibrissae of the California sea lion are similar in size, but less flattened than those of a harbor seal, and do not share the undulated structure. The Reynolds number was based on the vibrissa diameter taken approximately 5 mm from the base using the mean of the two ellipse semi-axes for both species and additionally averaged over the thick and thin undulation for the harbor seal. Re ranged from 186 to 340 for the harbor seal and from 284 to 535 for the sea lion vibrissae. Considering only the cases where the Re values differed by 5% or less, we found that the dynamic forces acting on the base of the harbor seal vibrissae were on average 6.2 times lower than

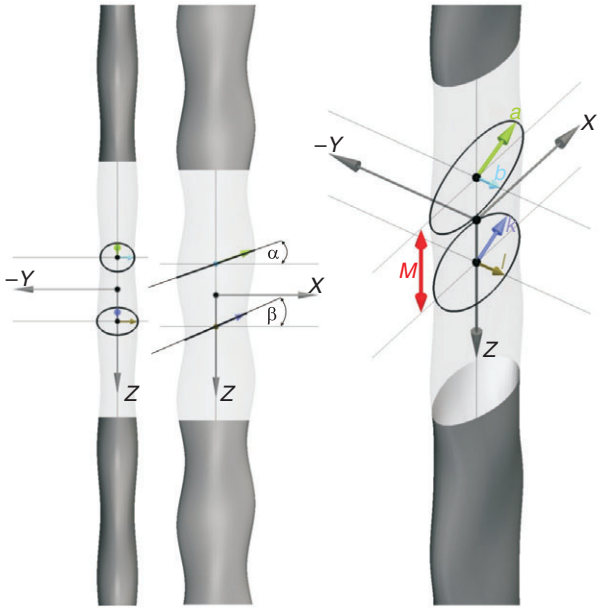

Fig. 4. Parameters of the idealized vibrissa surface model. *M*, the half-period of the undulation, equals 0.91 mm. *a* and *b*, the radii of the vibrissal cross-section in the laterally wide location, equal 0.595 mm and 0.24 mm, respectively. *k* and *l*, the radii of the vibrissal cross-section in the laterally narrow location, equal 0.475 mm and 0.29 mm, respectively. The connecting lines between the minima and maxima of the undulation on the rostral and caudal edges of the vibrissa, and thus the directions in which *a* and *k* were measured, were found not to be perpendicular to the vibrissal axis but oriented at angles α (15.27 deg) and β (17.60 deg), as indicated.

the forces acting on the vibrissae of the sea lion. Considering all flow speeds tested, the factor was 9.5.

The flow phenomena causing this effect were investigated using micro-stereo-PIV. For the PIV measurements, a harbor seal vibrissa with an average hydraulic diameter of 0.74 mm was used, resulting in *Re* values of approximately 300. An example of the time-averaged flow-field created from the entire set of 13 measurement planes is presented in Fig. 3. The 3-D streamlines show the formation of primary vortices as they occur also in the two-dimensional (2-D) vortex street behind a straight cylinder – but considerably altered by the 3-D vibrissa structures. The first indication of this effect can be taken from the curved layout of the vortex cores. Most significantly, however, the cross-correlation of the velocity fluctuations *u*' and *w*' given as the Reynolds stress, normalized with the velocity of the oncoming flow *U*, $\overline{u'w'}/U^2$ shows a strong deviation from zero, thus indicating fully 3-D flow structures, which include vortex segments with an orientation in the spanwise direction (*z*-direction; for definitions see Fig. 3).

To resolve the flow structures in more detail, CFD simulations of the flow around a harbor seal vibrissa were performed on a structured mesh with 8 million nodes around one single vibrissa. To generate a vibrissa surface model for the calculations, 13 different vibrissae with a total of 81 undulations were measured using photogrammetry. To characterize a typical vibrissa shape, we determined the four semi-axes of the two governing ellipses (*a*, *b*, *k*, *l*), the distance of the two ellipses (*M*) and the angles of attack (α, β) from each vibrissa. By averaging, an idealized vibrissa surface model was obtained (Fig. 4). Using DNS of the Navier–Stokes equations, 120,000 time-steps of the unsteady velocity vector and pressure distribution field were calculated, covering 100 cycles of

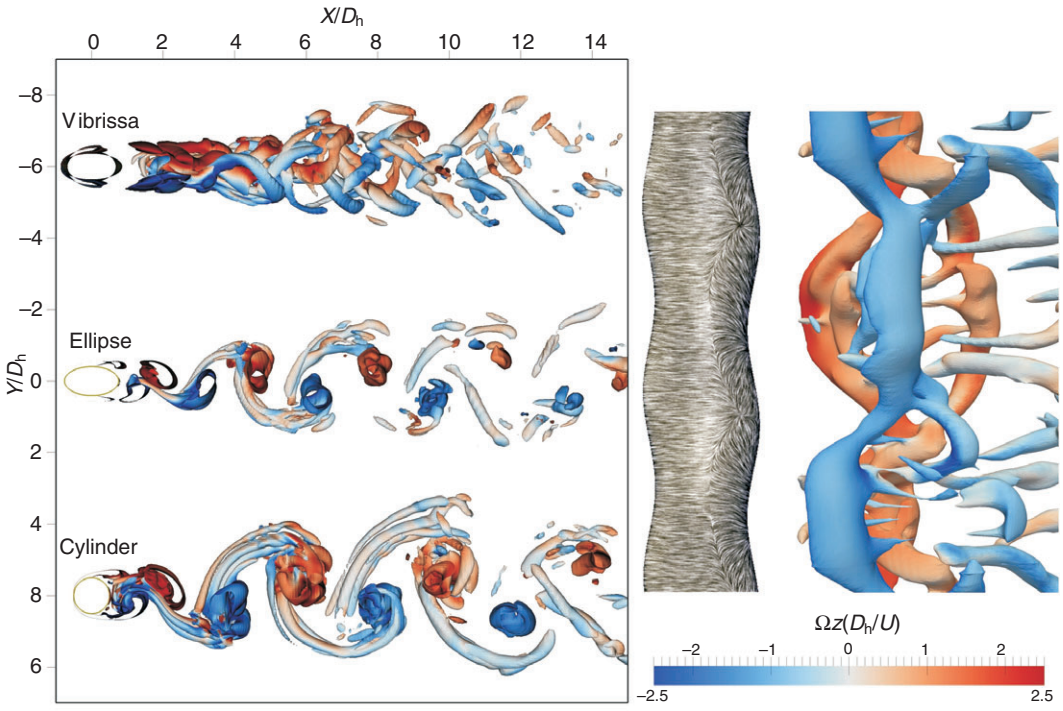

Fig. 5. Numerical simulation of the wake-flow behind different cylinder bodies at a *Re* of 500, vortex cores depicted as isosurfaces using the Q-criterion (Hunt et al., 1988; Jeong and Hussain, 1995). Color: cross-stream vorticity Ω_z. Left panel (top to bottom): wake behind a vibrissa of a harbor seal, behind a cylinder with elliptic cross-section and behind a circular cylinder. The radius ratio of the elliptic cylinder corresponds to the mean radius ratio along the vibrissa. Right panel: side view of the wake behind a vibrissa of a harbor seal. The surface flow pattern generated using the LIC technique (Cabral and Leedom, 1993) clearly indicates a wavy separation line along the axis of the vibrissa. Note that Fig. 5 shows instantaneous flow-fields, whereas the experimental results in Fig. 3 show a time-averaged flow-field.

the primary vortex separation period. The numerically calculated Reynolds stresses of the idealized vibrissa fell within ±30% of the experimental values from the micro-stereo-PIV. Fig. 5 shows a vortex core reconstruction from one instantaneous time-step for a vibrissa in comparison with those from a circular as well as an elliptic cylinder (radius ratio of the elliptic cylinder corresponds to the mean radius ratio along the vibrissa). Vortex cores are depicted as isosurfaces using the Q-criterion (Jeong and Hussain, 1995). The wake flow-field for the vibrissa (top) differs considerably from that of the comparison cylinders. Neither can large-scale primary vortex structures be found in the wake of the vibrissa nor are the vortex structures stable over a significant downstream distance, as they are for a circular cylinder (Brede et al., 1996). Analyzing the 3-D structure of the wake of the vibrissa (Fig. 5, right), we find that the separation of primary vortices (Kármán vortices) is replaced by a complex 3-D vortex structure in which various states of vortex separation occur simultaneously on different locations in a spanwise direction. Furthermore, the region of vortex formation is considerably shifted downstream compared with the circular or elliptic cylinder wake, thus opening a gap between the vibrissa surface and the region with fluctuating flow (Figs 5, 6). Therefore, the resulting pressure imposed on the complete vibrissa is more symmetric compared with that on a circular or an elliptic cylinder. The three features together – the reduction of the primary vortex separation, the gap between the vibrissa and the first vortices and the symmetry of the pressure field – prevent large periodic forces on the vibrissa originating from its own wake and thus prevent vortex-induced vibrations. As a result, lift forces on the vibrissa calculated from CFD data are reduced by more than 90% (Fig. 7), and the mean drag force is reduced by approximately 40% (Fig. 8) compared with those on a circular cylinder with an identical hydraulic diameter.

DISCUSSION

Comparison of the experimental and computational results

The experimental and computational results from this study are in good agreement and yield a coherent picture. Both the recordings of the vibrissa of a harbor seal performing a hydrodynamic localization task while using a head-mounted-camera and the force measurements on vibrissae in a rotational flow tank have demonstrated that harbor seal vibrissae are able to glide smoothly through the water. They are subjected to significantly lower hydrodynamic forces than a circular cylinder or a sea lion vibrissa at the same *Re* value. Micro-stereo-PIV results revealed 3-D flow structures and a spanwise exchange of momentum. CFD calculations have resolved the flow in more detail and indicated a reduction of the standard deviation of the lift and drag forces of approximately 90% on the harbor seal vibrissa as compared with those on a circular cylinder. This amount of reduction is in good accordance with the experimental results on vibrissae of harbor seals (undulated) compared with those of sea lions (not undulated) obtained in the rotational flow tank. Comparing the numerically calculated Reynolds-stresses with the results from the micro-stereo-PIV experiments, the numerical results fell within ±30% of the experimental values. This is a satisfying result considering that the difference includes not only the imaging noise but also the geometrical variations of the individual vibrissa compared with the idealized vibrissa CFD model, and it provides an additional validation of the CFD scheme. As a result, we conclude that few or no vortex-induced vibrations occur on harbor seal vibrissae owing to the effective suppression of the periodic forces.

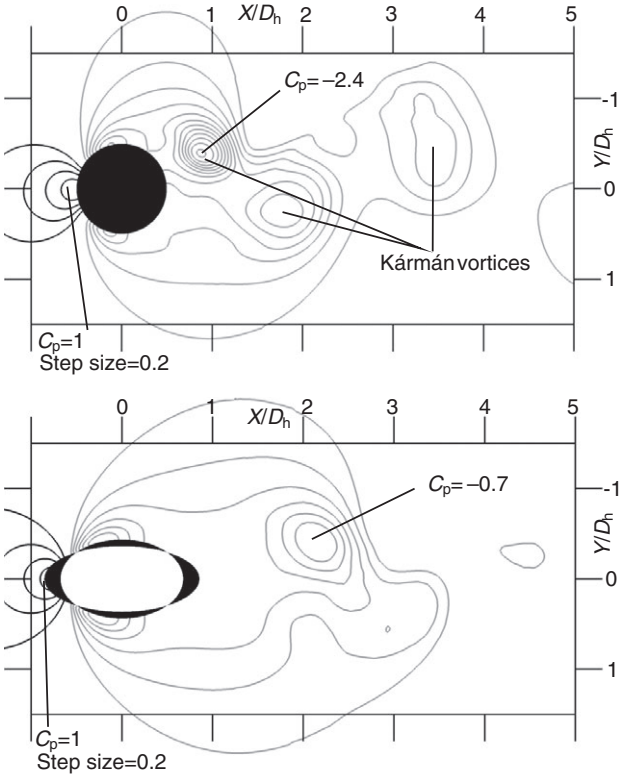

Fig. 6. Instantaneous contour lines of the pressure coefficient:

$$C_p = \frac{2(p - P)}{\rho U^2},$$

where p represents the local pressure, P indicates the free-stream pressure, U is the free-stream velocity and ρ is the fluid density. Top: infinite cylinder Re=500, C_p minimum=–2.4, step size=0.2. bottom: vibrissa Re=500, C_p minimum=–0.7, step size=0.2.

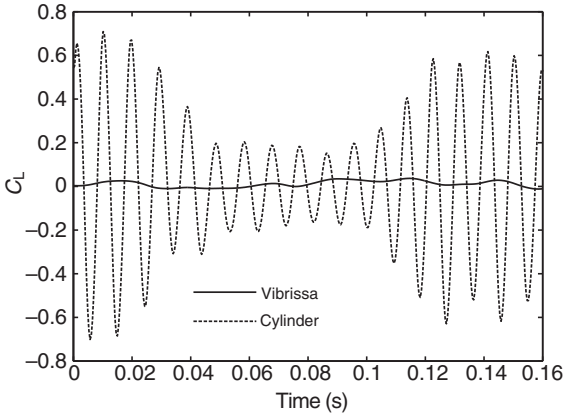

Fig. 7. Time-history of the lift coefficient:

$$C_L = \frac{2F_L}{\rho U^2 A},$$

where F_L represents the total lift force, ρ the fluid density, U the free-stream velocity and A indicates the projected area in the free-stream direction. The solid line shows the result for the vibrissa, the dashed line for the cylinder.

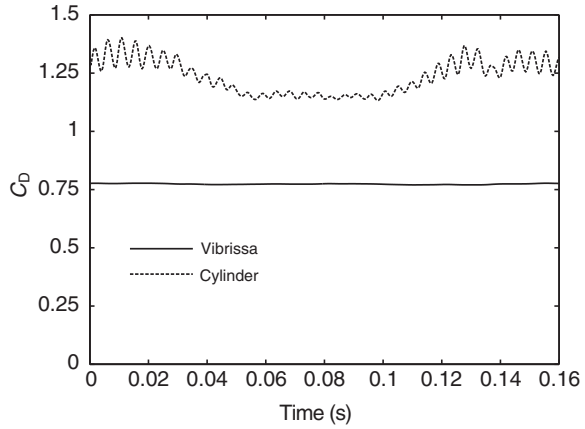

Fig. 8. Time-history of the drag coefficient:

$$C_D = \frac{2F_D}{\rho U^2 A},$$

where F_D represents the total drag force, ρ the fluid density, U the free-stream velocity and A indicates the projected area in the free-stream direction. The solid line shows the result for the vibrissa, the dashed line for the cylinder.

Role of the vortex suppression in the sensory biology of the harbor seal

Harbor seals have been shown to use their vibrissae for the detection of water movements not only in a sit-and-wait strategy (Dehnhardt et al., 1998a) but also while swimming forwards (Dehnhardt et al., 2001). It has been hypothesized that harbor seal whiskers might vibrate in the flow during forward swimming owing to vortex-induced vibrations and that the actual signal detected by the seal might consist of the modulations of these vibrations owing to biologically relevant hydrodynamic events such as those caused by swimming prey (Dehnhardt et al., 2001). Here we show that harbor seal vibrissae have evolved a structure that largely reduces vortex-induced vibrations. We conclude that the seals, by reducing these vibrations, keep their vibrissae as still as possible while searching for, or detecting, relevant hydrodynamic signals and thus enhance the signal-to-noise ratio (cf. Fish et al., 2008). A similar vibrissal structure is present in 15 out of the 18 species of true seals (*Phocidae*), demonstrating the high adaptive value of the effects described here.

The sensory threshold of the harbor seal vibrissal system for water movements lies at a velocity as low as 0.25 mm s^{-1}, representing a displacement length below 1 μm, measured for the best frequency of 50 Hz. This result was obtained from tests with the seal at rest and hydrodynamic stimuli produced with an oscillating sphere (Dehnhardt et al., 1998a). Renouf (Renouf, 1979) and Mills and Renouf (Mills and Renouf, 1986) performed behavioral experiments in which the vibrissae of harbor seals were stimulated by a vibrating rod in air. They found that the sensitivity in terms of displacement was over 100 times lower at 50 Hz than in the underwater experiments performed by Dehnhardt et al. (Dehnhardt et al., 1998a) and increased from 50 to 1000 Hz. However, the signal transduction in air depends on how many vibrissae touched the stimulator and at which points along the span (no details are given). Therefore, the results from the underwater experiments by Dehnhardt et al. (Dehnhardt et al., 1998a), which are also consistent with electrophysiological studies (Dykes, 1975), appear more relevant to the present discussion. Thus, the vibrissal system of harbor seals must be considered extremely sensitive at frequencies between 10 and 100 Hz, matching the properties of the hydrodynamic signals generated by prey fish (Bleckmann et al., 1991; Hanke and Bleckmann, 2004). Unfortunately, the frequency of the vortex shedding (f) from a cylindrical vibrissa at the swim speed of the harbor seal would lie in the same range: calculated from Strouhal's empirical formula $f=U/d\times0.198(1–19.7/Re)$ (Douglas et al., 1979), the vortex shedding frequency is 95 Hz for a 1 mm diameter cylinder at a swim speed of 0.5 m s^{-1}. The frequencies of vortex-induced vibrations would overlap with the operational range of the sensory system if the vibrissa had a circular cross-section, and therefore their suppression is crucial.

Vortex suppression by wavy surfaces

Vortex-induced vibrations and strategies to reduce them have been the subject of extensive studies in engineering (Bearman and Owen, 1998; Owen et al., 2001; Owen et al., 2000; Scruton, 1965; Williamson and Govardhan, 2004; Williamson and Govardhan, 2008; Zdravkovich, 1981). Much of the recent interest originates from offshore industries (Bearman, 2009). Many devices for vortex suppression, among them the most widely used helical strakes (Scruton, 1965), have the disadvantage that they increase the drag. Four types of cylinder-like objects with wavy surfaces have been presented previously, all of which reduce the drag: (a) cylinders with half-ellipse cross-section featuring wavy trailing edges (Tombazis and Bearman, 1997); (b) cylinders with rectangular cross-section featuring wavy leading edges (Bearman and Owen, 1998); (c) cylinders with a circular cross-section and a sinusoidal axis (Owen et al., 2001; Owen et al., 2000) and, to avoid directional characteristics, (d) cylinders with a circular cross-section employing bumps at alternating angles (Owen et al., 2001). Regular Kármán vortex shedding that causes vortex-induced vibration was substantially suppressed for types (b–d) and was at least reduced for type (a). For types (a) and (b), a drag reduction of up to 30% was found, which is remarkably close to the 40% drag reduction found in our study. However, the drag is generally higher on cylinders with rectangular cross-section than on those with circular cross-section and is higher on blunt than on rounded trailing edges. So, in absolute terms, the drag was still higher on objects (a) and (b) than on a comparable vibrissa. The type (c) design resulted in the best drag reduction of all objects tested (up to 47%) as long as the plane of the waviness was parallel to the flow (zero angle of attack). Flow visualization (Owen et al., 2000) showed that the Kármán vortex shedding was suppressed and replaced by the shedding of more symmetrical vortices and that there was a periodic variation of the wake width across the span. Both features are also present in the wake behind the vibrissa and appear to be caused by the wavy separation line (cf. Fig. 5, right), which is a common characteristic of these flows. The wavy leading edge is the feature shared by all objects that suppressed vortex-induced vibrations, including the vibrissae of the harbor seal.

Wavy surfaces in nature

In nature, morphological structures that suppress vortex-induced vibrations, as reported here, were unknown to date. The flippers of humpback whales (*Megaptera novaeangliae*) share the feature of a wavy leading edge that influences the flow (Fish and Battle, 1995; Fish et al., 2008; Fish and Lauder, 2006; Miklosovic et al., 2004). The bumps or tubercles on the leading edge of the flippers of a humpback whale have been shown to delay stall and increase hydrodynamic efficiency (i.e. the ratio of lift coefficient to drag coefficient) at moderate to high angles of attack and to reduce the drag at moderate angles of attack (Fish et al., 2008; Miklosovic

et al., 2004; Watts and Fish, 2001). Interestingly, no drag reduction was found at zero angle of attack (Miklosovic et al., 2004). Humpback whales use their flippers to perform extremely sharp turns at high speed during the pursuit of prey (Hain et al., 1982). The delay of stall and the increase of hydrodynamic efficiency in these maneuvers are believed to be the reason for the tubercles on the flippers of humpback whales (Fish et al., 2008; Miklosovic et al., 2004).

Future directions

The effect of different angles of attack, as studied in the flippers of humpback whales, would also be of interest in the vibrissae of harbor seals. The flow around a vibrissa, contrary to the flow around a humpback whale flipper, is never steady and always shows a separation line. Typical stall – the permanent detachment of the flow from the surface – does not occur in the case of the vibrissa flow. It would, however, be useful to maintain the suppression of vortex-induced vibrations over a certain range of angles of attack because the angle might change owing to head movements or flow gradients in the environment. For the future, we need to study the effects of different angles of attack.

The mechanical properties of the mounting of the vibrissa – i.e. the follicle–sinus complex and specifically the sinuses that surround the hair shaft – are largely unknown to date. As the damping of the mounting of a cylinder-like object plays a crucial role in its behavior in the flow (Klamo et al., 2006), we plan to measure the mechanical characteristics of the follicle–sinus complex and the vibrissa *in vivo*. Qualitative observations show that the mounting in the follicle–sinus complex further damps potential oscillations of the vibrissa as compared with a rigid mount and contributes to the suppression of vortex-induced vibrations.

The structure of the harbor seal vibrissa demonstrates a highly efficient mechanism for the suppression of forces owing to vortex shedding from rod-like objects with drag reduction. Numerous applications in biomimetic designs are conceivable, including flow sensors for underwater vehicles or parts of buildings and offshore facilities with reduced vibrations from wind or water flow. Inspiration from nature has so far been lacking in this field of research. Particularly challenging is the suppression of vortex-induced vibrations in flexible structures with low mass (Owen et al., 2001), as observed here. Future studies will focus on both the hydrodynamics of harbor seal vibrissae with regard to their role in the sensory biology of the animal and on the transfer of the findings into technical applications.

LIST OF SYMBOLS AND ABBREVIATIONS

A	projected area in free-stream direction
C_D	drag coefficient
C_L	lift coefficient
C_p	pressure coefficient
d	cylinder diameter
D_h	hydraulic diameter
f	frequency of vortex shedding
F_D	drag force
F_L	lift force
HMC	head-mounted camera
p	pressure
P	free-stream pressure
ρ	fluid density
Re	Reynolds number
U	velocity of the oncoming flow
u'	water velocity fluctuation in the U direction
w'	water velocity fluctuation perpendicular to u'
Ω_z	cross-stream vorticity

ACKNOWLEDGEMENTS

We thank Cansu Aslan for help with the head-mounted camera recordings. Andreas Stein (Institute of Human Genetics, Bonn, Germany) photographed Fig. 1. This study was supported by grants of the German Research Foundation (SPP 1207) to G.D., M.B., W.H. and A.L., and the Volkswagenstiftung to G.D.

REFERENCES

Adrian, R. J. (1991). Particle imaging techniques for experimental fluid mechanics. *Annu. Rev. Fluid Mech.* **23**, 261-304.

Balachandar, S., Mittal, R. and Najjar, F. M. (1997). Properties of the mean recirculation region in the wakes of two-dimensional bluff bodies. *J. Fluid Mech.* **351**, 167-199.

Bearman, P. W. (2009). Understanding and predicting vortex-induced vibrations. *J. Fluid Mech.* **634**, 1-4.

Bearman, P. W. and Owen, J. C. (1998). Reduction of bluff-body drag and suppression of vortex shedding by the introduction of wavy separation lines. *J. Fluids Struct.* **12**, 123-130.

Bleckmann, H., Breithaupt, T., Blickhan, R. and Tautz, J. (1991). The time course and frequency content of hydrodynamic events caused by moving fish, frogs, and crustaceans. *J. Comp. Physiol. A* **168**, 749-757.

Brede, M., Eckelmann, H. and Rockwell, D. (1996). On secondary vortices in the cylinder wake. *Phys. Fluids* **8**, 2117-2124.

Brede, M., Witte, M. and Leder, A. (2006). Stereo-Micro PIV measurements of the three-dimensional separated flow in the wake of a backward facing step. In *Proceedings of the 13th International Symposium on Applications of Laser Techniques to Fluid Mechanics*. Lisbon: Calouste Gulbenkian Foundation.

Cabral, B. and Leedom, L. (1993). Imaging Vector Fields Using Line Integral Convolution. In *International Conference on Computer Graphics and Interactive Techniques: Proceedings of the 20th annual conference on Computer graphics and interactive techniques*, pp. 263-270.

Catania, K. C., Hare, J. F. and Campbell, K. L. (2008). Water shrews detect movement, shape, and smell to find prey underwater. *Proc. Natl. Acad. Sci. USA* **105**, 571-576.

Dehnhardt, G. (2002). Sensory systems. In *Marine Mammal Biology* (ed. A. R. Hoelzel), pp. 116-141. Oxford: Blackwell Publishing.

Dehnhardt, G. and Kaminski, A. (1995). Sensitivity of the mystacial vibrissae of harbour seals (*Phoca vitulina*) for size differences of actively touched objects. *J. Exp. Biol.* **198**, 2317-2323.

Dehnhardt, G., Mauck, B. and Bleckmann, H. (1998a). Seal whiskers detect water movements. *Nature* **394**, 235-236.

Dehnhardt, G., Mauck, B. and Hyvärinen, H. (1998b). Ambient temperature does not affect the tactile sensitivity of mystacial vibrissae of harbour seals. *J. Exp. Biol.* **201**, 3023-3029.

Dehnhardt, G., Hyvärinen, H., Palviainen, A. and Klauer, G. (1999). Structure and innervation of the vibrissal follicle-sinus complex in the Australian water rat, *Hydromys chrysogaster*. *J. Comp. Neurol.* **411**, 550-562.

Dehnhardt, G., Mauck, B., Hanke, W. and Bleckmann, H. (2001). Hydrodynamic trail following in harbor seals (*Phoca vitulina*). *Science* **293**, 102-104.

Douglas, J. F., Gasiorek, J. M. and Swaffield, J. A. (1979). *Fluid Mechanics.* London: Pitman Publishing.

Dykes, R. W. (1975). Afferent fibers from mystacial vibrissae of cats and seals. *J. Neurophysiol.* **38**, 650-662.

Ebara, S., Kumamoto, K., Matsuura, T., Mazurkiewicz, J. E. and Rice, F. L. (2002). Similarities and differences in the innervation of mystacial vibrissal follicle-sinus complexes in the rat and cat: A confocal microscopic study. *J. Comp. Neurol.* **449**, 103-119.

Fish, F. E. and Battle, J. M. (1995). Hydrodynamic design of the humpback whale flipper. *J. Morphol.* **225**, 51-60.

Fish, F. E. and Lauder, G. V. (2006). Passive and active flow control by swimming fishes and mammals. *Annu. Rev. Fluid Mech.* **38**, 193-224.

Fish, F. E., Howle, L. E. and Murray, M. M. (2008). Hydrodynamic flow control in marine mammals. *Integr. Comp. Biol.* **48**, 788-800.

Hain, J. H. W., Carter, G. R., Kraus, S. D., Mayo, C. A. and Winn, H. E. (1982). Feeding behavior of the humpback whale, *Megaptera novaeangliae*, in the western north-atlantic. *Fish. Bull.* **80**, 259-268.

Hanke, W. and Bleckmann, H. (2004). The hydrodynamic trails of Lepomis gibbosus (Centrarchidae), Colomesus psittacus (Tetraodontidae) and Thysochromis ansorgii (Cichlidae) measured with Scanning Particle Image Velocimetry. *J. Exp. Biol.* **207**, 1585-1596.

Hanke, W., Brücker, C. and Bleckmann, H. (2000). The ageing of the low-frequency water disturbances caused by swimming goldfish and its possible relevance to prey detection. *J. Exp. Biol.* **203**, 1193-1200.

Hartmann, M. J. (2001). Active sensing capabilities of the rat whisker system. *Auton. Robots* **11**, 249-254.

Hunt, J. C. R., Wray, A. A. and Moin, P. (1988). Eddies, streams, and convergence zones in turbulent flows. In *Center for Turbulence Research: Proceedings of the Summer Program*, pp. 193.

Jeong, J. and Hussain, F. (1995). On the identification of a vortex. *J. Fluid Mech.* **285**, 69-94.

Klamo, J. T., Leonard, A. and Roshko, A. (2006). The effects of damping on the amplitude and frequency response of a freely vibrating cylinder in cross-flow. *J. Fluids Struct.* **22**, 845-856.

Leder, A. (1991). Dynamics of fluid mixing in separated flows. *Phys. Fluids A* **3**, 1741-1748.

Miklosovic, D. S., Murray, M. M., Howle, L. E. and Fish, F. E. (2004). Leading-edge tubercles delay stall on humpback whale (Megaptera novaeangliae) flippers. *Phys. Fluids* **16**, L39-L42.

Mills, F. H. J. and Renouf, D. (1986). Determination of the vibration sensitivity of harbour seal *Phoca vitulina* (L.) vibrissae. *J. Exp. Mar. Biol. Ecol.* **100**, 3-9.
Nguyen, N.-T. and Wereley, S. T. (2002). *Fundamentals and Applications of Microfluidics*. Boston: Artec House.
Owen, J. C., Szewczyk, A. A. and Bearman, P. W. (2000). Suppression of Kármán vortex shedding. Gallery of Fluid Motion. *Phys. Fluids* **12**, S9.
Owen, J. C., Bearman, P. W. and Szewczyk, A. A. (2001). Passive control of VIV with drag reduction. *J. Fluids Struct.* **15**, 597-605.
Prasad, A. K. and Adrian, R. J. (1993). Stereoscopic particle image velocimetry applied to liquid flows. *Exp. Fluids* **15**, 49-60.
Renouf, D. (1979). Preliminary measurements of the sensitivity of the vibrissae of Harbour seals (*Phoca vitulina*) to low frequency vibrations. *J. Zool.* **188**, 443-450.
Schulte-Pelkum, N., Wieskotten, S., Hanke, W., Dehnhardt, G. and Mauck, B. (2007). Tracking of biogenic hydrodynamic trails in a harbor seal (Phoca vitulina). *J. Exp. Biol.* **210**, 781-787.
Scruton, C. (1965). On the wind-excited oscillations of stacks, towers and masts. In *Proceedings of the Symposium on Wind Effects on Buildings and Structures,* pp. 798-836. London: HMSO.
Tombazis, N. and Bearman, P. W. (1997). A study of three-dimensional aspects of vortex shedding from a bluff body with a mild geometric disturbance. *J. Fluid Mech.* **330**, 85-112.
Watts, P. and Fish, F. E. (2001). The influence of passive, leading edge tubercles on wing performance. In *Proceedings of the Twelfth International Symposium on Unmanned Untethered Submers. Technol.* Durham, NC: Autonomous Undersea Systems Institute.
Williamson, C. H. K. and Govardhan, R. (2004). Vortex-induced vibrations. *Annu. Rev. Fluid Mech.* **36**, 413-455.
Williamson, C. H. K. and Govardhan, R. (2008). A brief review of recent results in vortex-induced vibrations. *J. Wind Eng. Ind. Aerodyn.* **96**, 713-735.
Zdravkovich, M. M. (1981). Review and classification of various aerodynamic and hydrodynamic means for suppressing vortex shedding. *J. Wind Eng. Ind. Aerodyn.* **7**, 145-189.
Zdravkovich, M. M. (1995). *Flow Around Circular Cylinders*, Vol.1 (*Fundamentals*). Oxford: Oxford University Press.
Zdravkovich, M. M. (2003). *Flow Around Circular Cylinders*, Vol. 2 (*Applications*). Oxford: Oxford University Press.

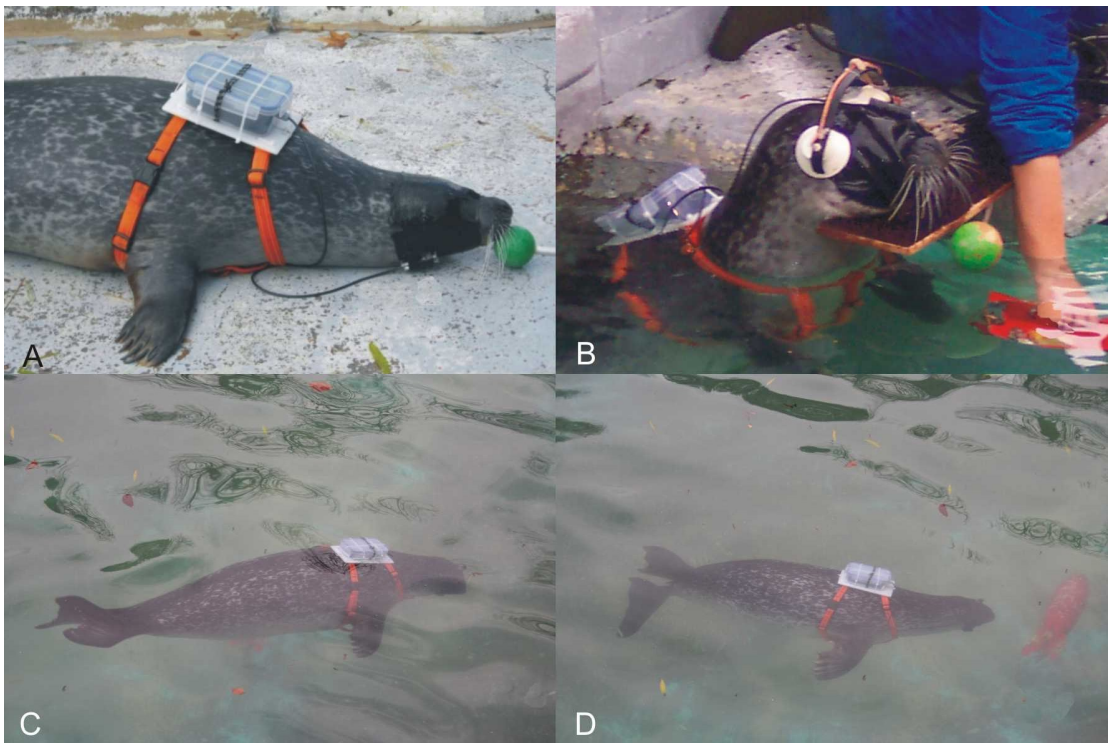

Figure S1. Experimental procedure for the head-mounted camera recordings. *A*, seal stationed on land wearing the eye-mask and the head-mounted camera (HMC) system . *B*, seal with HMC system stationed in the water waiting for the beginning of a trial. The seal's vibrissae are out of the water, and the seal is wearing headphones with pink noise in order to avoid secondary tactile and acoustic cues as long as the miniature submarine (red) is generating a hydrodynamic trail. *C*, seal with eye-mask and head-mounted camera system during hydrodynamic trail following. *D*, close to the completion of the task.

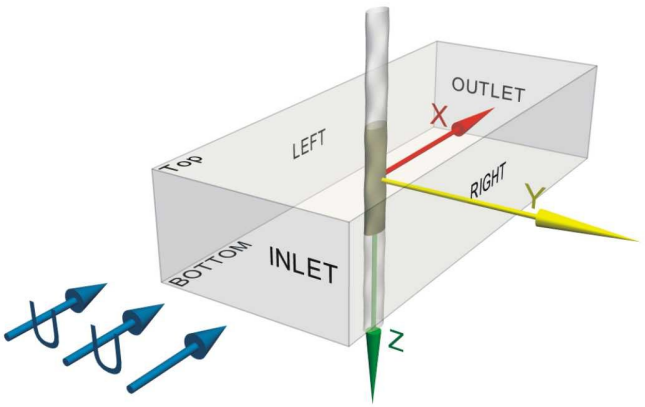

Figure S2: Parameters and computational domain for the numerical simulation.

computational domain:

$-10 \leq X/D_h \leq 15$

$-5 \leq Y/D_h \leq 5$

$-\pi/2 \leq Z/D_h \leq \pi/2$ for the cylinder

$-\pi/2 \leq Z/D_h \leq \pi/2$ for the ellipse

$-0.865\pi \leq Z/D_h \leq 0.865\pi$ for the vibrissa

boundary conditions:

Re = 500

LEFT & RIGHT: slip – condition

TOP-BOTTOM: periodic

INLET: $U = \frac{\mathrm{Re} \cdot u}{D_h}$

OUTLET: convective outlet; cylinder, ellipse and vibrissae: no slip surfaces

mesh parameters:

structured grid;o-grid topology around cylinder, ellipse and vibrissa;number of elements:

$8 \cdot 10^6$and $16 \cdot 10^6$